IMAGE-BASED FIELD OBSERVATION OF INFRAGRAVITY WAVES ALONG THE SWASH ZONE

Yoshimitsu Tajima[1]

This study develops an image-based monitoring techniques for observations of surf zone hydrodynamics especially focusing on evolution and propagations of infragravity waves along the coast. Laboratory experiment was first performed to investigate the relationship between image-captured shoreline fluctuations and recorded actual water surface fluctuations inside the surf zone. Frequency components of infragravity waves were extracted respectively from observed shoreline changes and recorded water surface fluctuations. Both components showed good agreement in terms of their alongshore distributions of phases and amplitudes. The same image-based technique was applied to the field, the Seisho coast when the typhoon 1112 approached the site and extracted infragravity wave components were found to be consistent with offshore wave data and showed characteristics of edge waves.

Keywords: image-based monitoring; swash zone; infragravity wave; edge wave

INTRODUCTION

Infragravity waves, amplified under stormy waves, may be one of important factors which determine coastal disaster characteristics. Tajima and Sato (2009), for instance, measured the inundation heights along the Seisho coast when the typhoon 0709 hit the coast in 2007 and pointed out that the measured alongshore distributions of the inundation heights showed clear periodic patterns in the alongshore direction and the length scale of this periodic pattern was much longer than the length of wind waves observed during the storm (Fig. 1). Tajima and Sato (2009) also showed that this observed periodic pattern of the inundation heights can be reasonably represented by a numerical wave model based on non-linear shallow water equations when incident wave conditions were given by those of infragravity waves with frequencies and directions specified from the observed offshore wave data
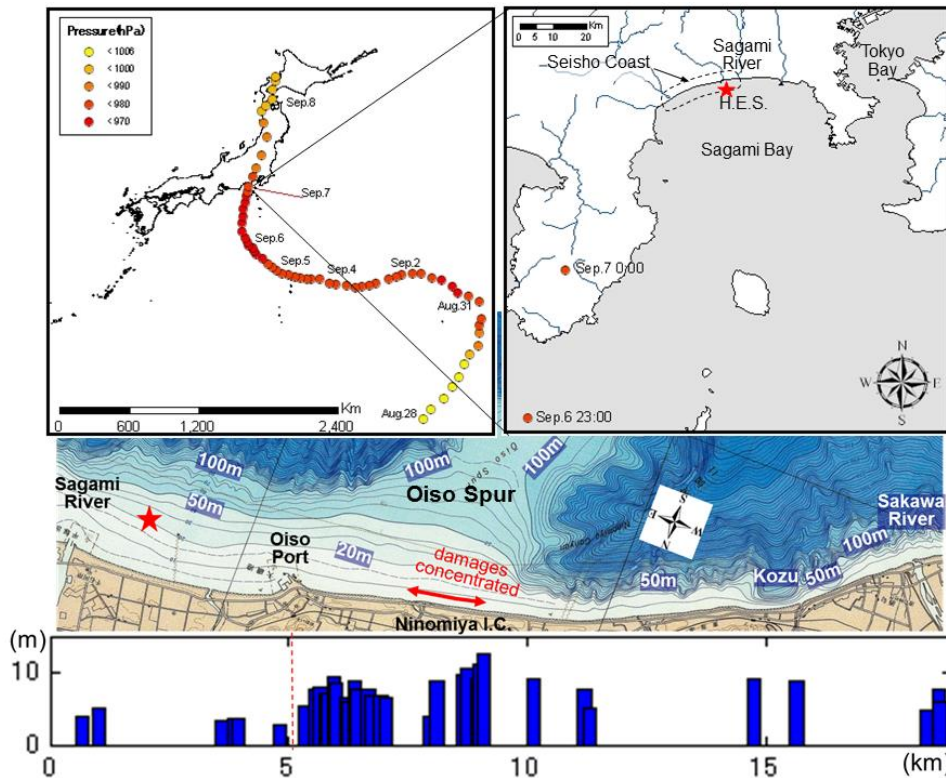

Figure 1 Track of Typhoon 0709 (top left), location of Seisho coast (top right) and alongshore distributions of measured inundation heights (middle and bottom). Middle and bottom figures are rotated and the star in the middle figure indicates the location of Hiratsuka Observation Station where wave data is recorded.

[1] Department of Civil Engineering, The University of Tokyo, Hongo 7-3-1, Bunkyo-ku, Tokyo, 113-8656, Japan

recorded near the focusing site.

A number of studies have focused on evolutions and behaviors of such infragravity waves induced by random waves. Janssen et al. (2003) and Seki and Mizuguchi (2008) investigated how the phase difference between infragravity waves and envelopes of random waves vary in the cross-shore direction through the numerical analysis and laboratory experiments of the one dimensional wave flume. Tajima and Sato (2010) carried out the laboratory experiments on the two dimensional basin and investigated how wave heights are locally concentrated when group waves with slowly varying envelopes were incident on the bathymetry where two bottom plane panels with different cross-shore slopes were attached with each other in the middle of the basin and a straight vertical seawall was placed along the shore. Ranasinghe et al. (2011) carried out the similar experiments to those of Tajima and Sato (2010) and also tested the applicability of Boussinesq-type non-linear dispersive wave model for predictions of such wave concentrations.

While there are a number of related studies, most of these existing studies are based either on laboratory experiments or on numerical analysis and relatively few studies are based on the actual field data. Kato (1981), for instance, analyzed the succeeding aerial photographs of the swash zone along the Sendai coast of Japan and showed that edge wave components formed standing waves along the coast. Due to the difficulty of direct measurements of swash zone hydrodynamics using instruments such as wave gauges, little data of swash zone hydrodynamics have been obtained from the field.

This study aims to develop an image-based remote monitoring technique especially focusing on observations for behavior of infragravity waves around the swash zone under stormy wave conditions. Laboratory experiment is first carried out to investigate the validity and applicability of the present monitoring procedures and then the same methodologies are applied to the image data sets recorded at the Seisho coast when the stormy waves attacked the site.

LABORATORY EXPERIMENT

Laboratory experiment was first carried out to investigate the relationship between actual water surface fluctuations in the swash zone and shoreline fluctuations extracted from the succeeding photographs of the swash zone.

Experimental Setup

Following Tajima and Sato (2010), two plane panels with different cross-shore slopes were attached with each other in the center of the basin so that cross-shore line with abruptly changing water depth is created in the center of the basin (Fig. 2). On this bathymetry, group waves were obliquely incident with angle of 20 degree from the shore-normal direction. The group wave was generated as a combination of two periodic waves with slightly offset periods, i.e., T_1=1.111s and T_2=0.909s and identical wave heights of H_{in}=2cm, respectively. As shown in Fig. 2, eight wave gauges were installed inside the surf zone so that recorded synchronized data sets of water surface fluctuations capture the behavior of infragravity waves. The basin was filled with water dyed in blue and moving shoreline was recorded by digital video camera, which was installed around 2 meter above the shoreline and was directed downward so that the camera can capture the entire shoreline. The frame rate of of the video recording was 30Hz. Time intervals of the succeeding pictures captured by the field camera, discussed
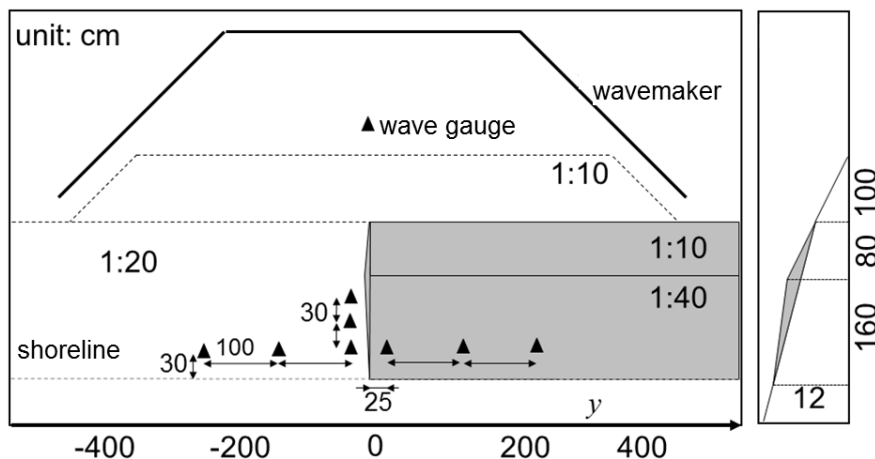

Figure 2 Setups of laboratory experiments. Triangles indicate locations of wave gauges.

later, was set to 0.6s. If a spatial scale of this experiment is assumed to be 1:100, the time scale in Froude's law is 1:10. Under this conditions, time interval of the images captured in the laboratory experiments, $\Delta t=1/30$s, corresponds to $\Delta t=1/3$s in the field scale. This time interval is reasonably consistent with actual time-intervals of the field camera, $\Delta t=0.6$s.

Image Analysis

The recorded images were first rectified based on horizontal X-Y coordinates on the sloping plane bed. Eight reference points with known coordinates were used for the image rectifications. As shown in Fig. 2, X and Y axis were respectively defined in the shoreward cross-shore direction and in the shore-parallel direction. Fig. 3 shows an example of original image and rectified image. Fig. 4 shows the time-variation of the shoreline locations at fixed Y-coordinate, Y=200cm. In this figure, vertical pixel coordinate corresponds to X-coordinates while horizontal pixel coordinates indicate the time after initiation of the video recording. In this figure, RGB values along the vertical line at Y=200cm were first extracted from rectified images and extracted line data from different images were placed one by one in the horizontal direction. Spatial and time scale of the image are shown in Fig. 4 and, as seen in Fig. 4, periodic fluctuations of the shoreline appear to have two different frequency components, i.e., the one around 1s and the other around 5s. The higher frequency corresponds to that of incident waves while the lower frequency corresponds to that of envelopes of the incident group waves.

Since the frequency of bound or free infragravity waves induced by group waves should be identical to that of envelopes of group waves, we need to distinguish which features dominantly caused the observed low-frequency shoreline fluctuations. Fig. 6 thus compares alongshore distributions of
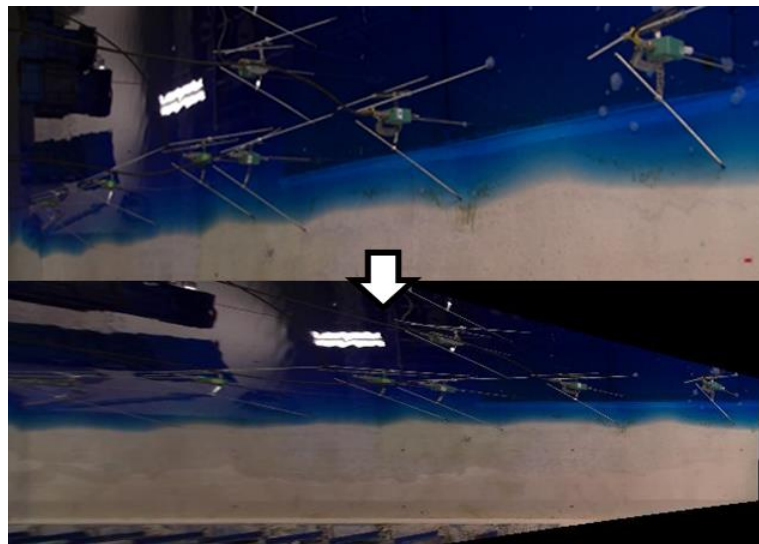

Figure 3 Examples of captured original image (top) and rectified image (bottom).
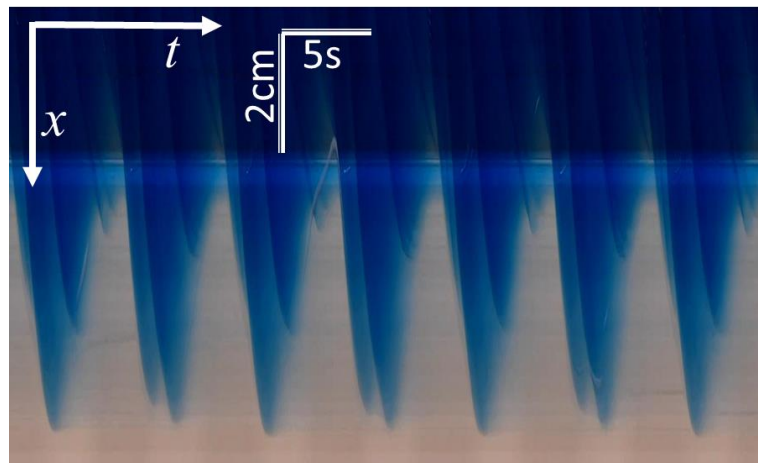

Figure 4 Time-varying cross-shore line images at fixed alongshore coordinate, y=200cm.

amplitude and phase difference of either shoreline or water surface fluctuations of infragravity wave components. In the figure, observed or recorded fluctuations of shoreline or water surface were first filtered to exclude short wave components with period of less than 2s. Following List (1992), envelope profiles of the recorded water surface fluctuations were also extracted and amplitude and phase relationships of obtained envelopes were also plotted in Fig. 6. As seen in Fig. 6, characteristics of observed shoreline fluctuations agree better with those of infragravity wave components of water surface fluctuations rather than those of envelope profiles of the group waves.

Observed alongshore distributions of the phase appears to linearly decrease with alongshore distance while there is a clear phase gap at the boundary between steeper and milder plane slopes. Linearly decreasing phase indicates that observed infragravity wave component propagate in the negative alongshore direction. It is also seen that the slope of these linearly decreasing phase is steeper
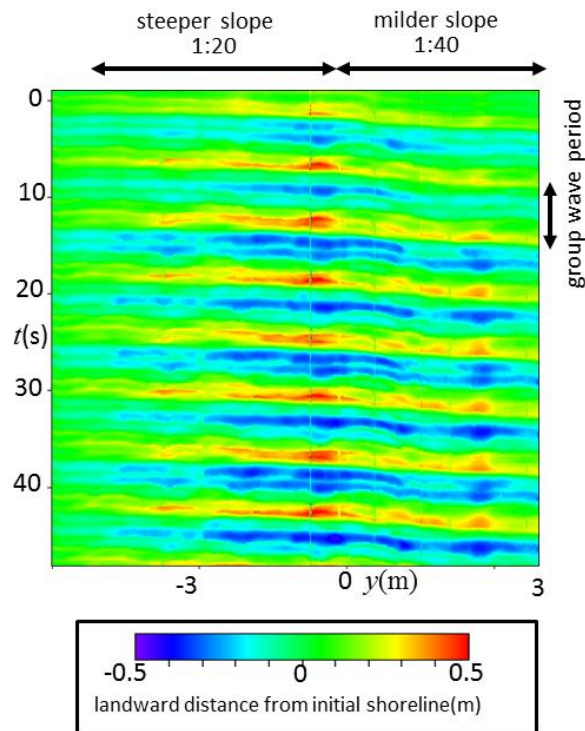

Figure 5 Extracted shoreline fluctuations(color) in time (vertical) and alongshore (horizontal) domains.
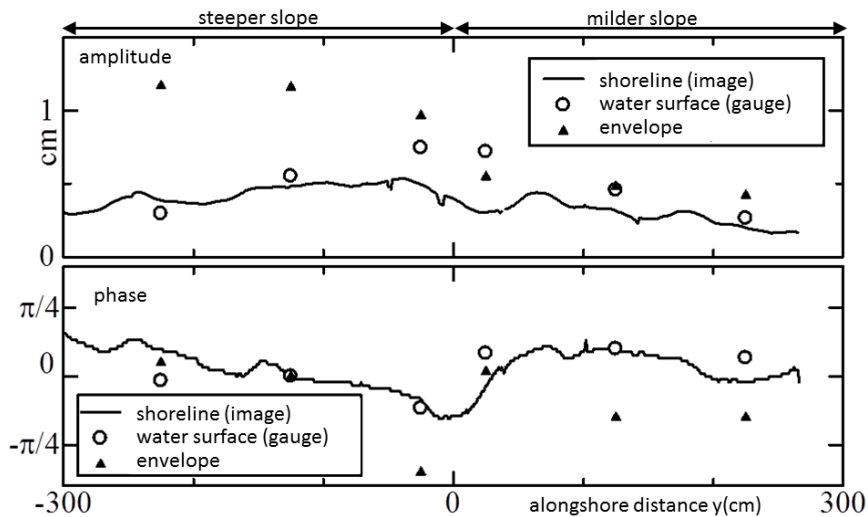

Figure 6 Alongshore distributions of amplitude (top) and phase (bottom) of fluctuations of low frequency components of: (i) shoreline fluctuations extracted from images (solid line); (ii) water surface fluctuations recorded by wave gauges (circle); and (iii) envelope of surface water fluctuations (triangle).

in front of the steeper plane slope compared to the one in front of the milder slope. This feature indicates that propagation speed of infragravity wave in the alongshore direction is faster along the steeper beach slope. This feature is consistent with the characteristics of edge waves while further analysis with other similar experimental cases should be needed to further understand the wave characteristics around the boundary of two different plane slopes.

FIELD APPLICATION

The same procedures of image-based observation of moving shoreline were applied to the Seisho coast. As shown in Fig. 1, Seisho coast is located in the middle of Sagami Bay, along the Pacific Coast of Japan. Seisho coast had suffered severe wave attacks and a part of highway along the coast was collapsed by stormy waves when typhoon 0709 hit the Pacific Coast of Japan in September 2007. While the coast has relatively long straight beach, cross-shore beach slope suddenly changes at the Oiso spur and measured inundation heights after the storm showed clear periodic fluctuations along the coast (Tajima and Sato, 2009). According to Sato et al. (1998), severely damaged area under the stormy waves due to the Typhoon 9720 in the year of 1997 were also concentrated around the Oiso spur.

Outline of Field Monitoring along Seisho Coast

A field camera was installed at west side of Oiso fishery port and images of swash zone along the coast were captured with time intervals of 0.6s when the typhoon 1112 hit the Pacific Coast of Japan in September 2011. The location of the field camera was just west side of Oiso port where is around 3km east from the most damaged area during the disaster in 2007. As shown in Fig. 1, the area recorded by the field camera corresponds to the area where we observed the second peak of periodic fluctuations of inundation heights from the most damaged site.

In order to investigate the characteristics of shoreline behavior under the stormy waves, images of the same swash zone under the daily wave conditions were also recorded in December 2011. Fig. 7 shows examples of the recorded images under stormy wave and daily wave conditions, respectively. In December, coordinates of eight reference points in the images were also recorded. Based on these reference points expressed in local XY coordinates, all the images recorded in December were rectified. While the images recorded under the stormy waves in September were also captured by the same camera from nearly the same location and with nearly identical angles, these angles and locations are not exactly the same and thus the relationship between pixel coordinates and corresponding captured targets are slightly different between the images in December and September. Since reference points for image rectification could not be obtained under the stormy wave conditions, September images were first rectified to December images by matching several reference points found in both images and then rectified September images were further rectified based on the rectification parameters obtained for December images. Fig. 8 shows examples of rectified images of both September and December images shown in Fig. 7. Here XY-coordinates were rotated from the original North-South and East-West directions so that the coordinates are nearly parallel to the longshore and cross-shore directions, respectively. Since the swash zone was wider and located at higher elevation under the stormy wave conditions, rectified images under the stormy wave conditions shows the rectified images with wider range in the cross-shore directions. Since both of these September and December rectified figures are based on the same XY-coordinates, these images can now be compared to each other in a quantitative manner even though they were recorded under different conditions.

Time-varying shoreline locations were then extracted from these rectified images based on rotated XY-coordinates. As seen in Fig. 7 and Fig. 8, color and brightness of beach sand surface was much darker compared to that of whitish bright surf zone. Cross-shore distributions of the brightness of each pixel therefore enabled us to detect the boundary between swash water and dry sand bed surface at most of the entire alongshore ranges throughout the entire observation period. Some locations in some images however yield misdetection of the shore line locations because of some exceptional conditions such as: (i) swash water was partially left even after receding of the shoreline boundary; (ii) floating debris with bright color was left after receding of the shoreline; and (iii) people were walking around the shoreline. To avoid detection errors due to above mentioned reasons, this study took the following procedures for shoreline estimation: (i) Create rectified image based on rotated XY-coordinates with cross-shore and alongshore pixel sizes of 0.1m and 2m, respectively; (ii) Check brightness of all the pixels of all the rectified images for the entire observation period and create the rectified image of the highest brightness at each pixel; (iii) Based on the image created in (ii), draw the smooth continuous line along the boundary between high and low brightness, which corresponds to the alongshore line of
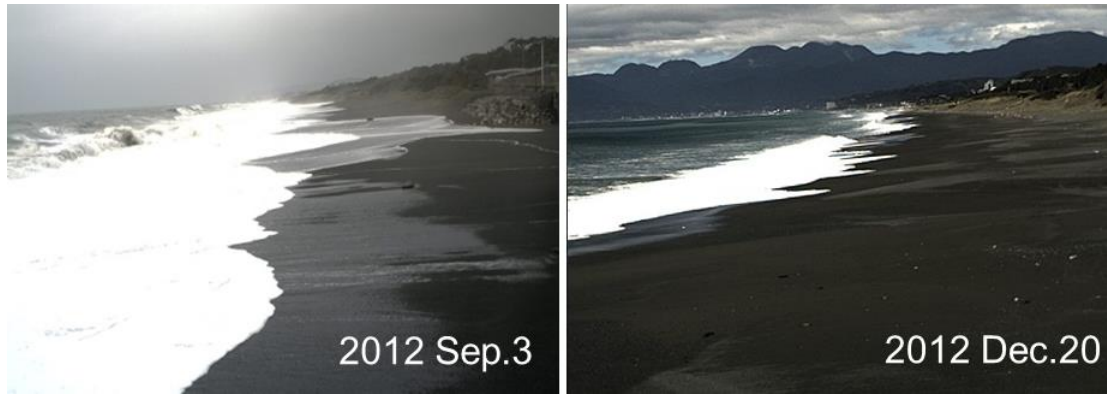
Figure 7 Examples of original images captured by a field camera under stormy waves (left, September) and daily waves (right, December).
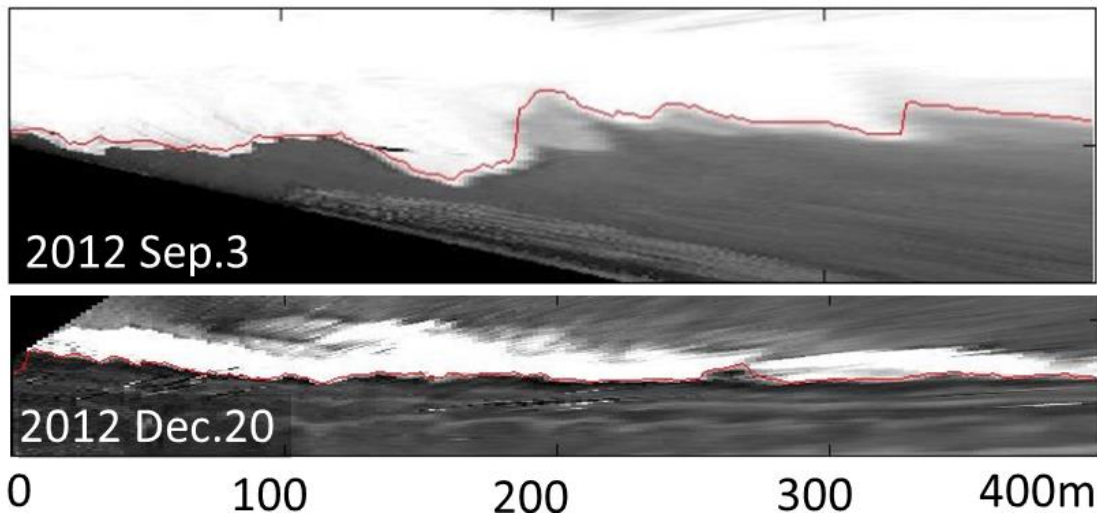

Figure 8 Examples of rectified images based on XY-coordinates parallel to the shoreline under stormy waves (top, September) and daily waves (bottom, December). Red solid lines indicate the extracted instantaneous shoreline profiles.

maximum runup height; (iv) Record the cross-shore coordinates along the line of maximum runup height at each alongshore pixel coordinate; (v) Starting from the obtained coordinates of maximum runup height, search land-water boundary in the seaward direction where pixel brightness abruptly increases; (vi) To avoid misdetection of actual shoreline locations, search several coordinates where such abrupt increase of the brightness is found; (vii) Compare several candidates of detected shoreline locations with those of alongshore neighbors and select the best combination of shoreline coordinates that yields the smoothest shoreline profile. Validity of these shoreline detection procedures was then tested by drawing extracted shoreline profiles on each of time-varying rectified images.

Analysis of Observed Swash Zone Characteristics

Above mentioned procedures were applied to obtained images and time-varying shoreline profiles were extracted. Extracted shoreline profile covers the alongshore stretch of around 400 meters with spatial alongshore intervals of 2m. Time interval of the extracted shoreline profiles is the same as the time interval of camera recording, i.e., Δt=0.6s. While the accuracy of the spatial estimation of the moving shoreline locations may be degraded as the distance from the camera to the target increases whereas spectral characteristics of shoreline movement should not be affected by the distance.

Fourier transform was respectively applied to the time-series of shoreline locations at each of alongshore grid and spatial map of obtained power spectral density was plotted as functions of frequency and alongshore locations. Fig. 9 compares color maps of estimated power spectral density of shoreline fluctuations in September and December. As seen in Fig.9, the values of estimated power spectral density are much larger in the case of stormy waves (September images) and it should be rather highlighted that distributions of power spectral density in September have several peaks in the range of

low frequency components less than f=1/30 (1/sec) whereas the ones in December under daily wave conditions have no such local peaks.

Fig. 10 compares power spectral density of shoreline fluctuations at three different alongshore locations and surface water fluctuations recorded at Hiratsuka Observation Station located around 1km
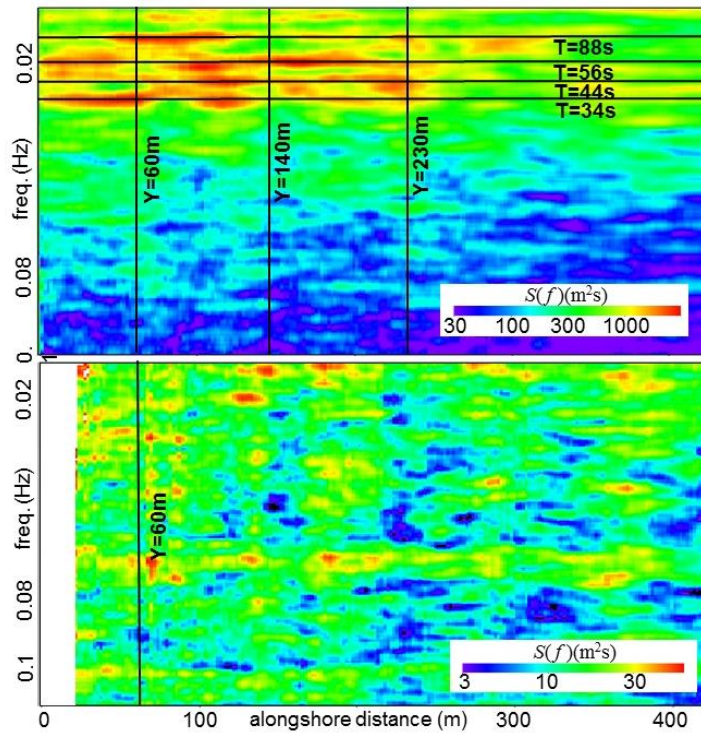

Figure 9 Distribution of power spectral density (in color) of observed shoreline fluctuations at different alongshore locations.
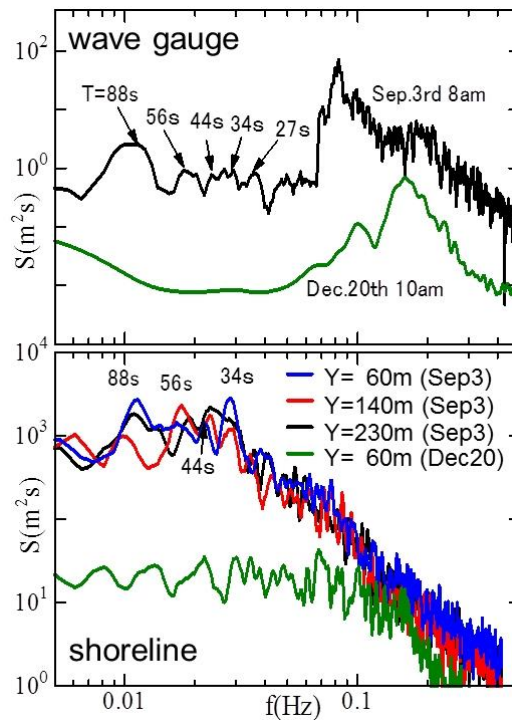

Figure 10 Power spectral density of: surface water fluctuations recorded at offshore Hiratsuka Observation Station (top) and shoreline fluctuations (bottom) both under stormy wave conditions (Sep.3) and daily wave conditions (Dec.20).

offshore of the target site with water depth of around 20m. Fig.10 shows power spectral density of water surface fluctuations recorded at Hiratsuka Observation Station both under stormy and daily wave conditions when images were recorded in September and December, respectively. As seen in the figure, peaks of power spectral density in the range of low frequency components are also found in those of water surface fluctuations and their peak frequencies surely match with each other under the stormy wave conditions. Under the daily wave conditions, on the other hand, peaks of low frequency components were not found both in shoreline and offshore water surface fluctuations. Offshore water surface fluctuations had several clear peaks in the frequency range higher than f (1/s)=1/30 whereas these peaks were not found in the power spectrum of observed shoreline fluctuations. High frequency components may be dissipated due to wave breakings in the surf zone.

As seen in Figs. 9 and 10, peaks of shoreline fluctuations in low frequency range appear to have certain periodic variations in the alongshore directions and alongshore distance of these periodic patterns appear to increase as corresponding wave period increases. This feature may suggest that infragravity waves might have formed partial standing waves in the alongshore directions. In order to further investigate the behavior of these infragravity wave components, Fig. 11 compares the alongshore distributions of amplitude and phase of shoreline fluctuations of specific frequency components at which peaks of power spectral density were found. In the frequency component of T=88s, the phase abruptly changes at Y=180m and the phase gap was around π. This feature clearly indicates that the infragravity wave components formed standing waves in the alongshore directions. In the case of frequency components of T=51s, on the other hand, the estimated phase varies linearly in the alongshore direction and thus infragravity wave of this frequency component behaves as progressive waves in the alongshore direction. Frequency components of T=56s shows step-like phase variations which may correspond to features of partial standing waves. In contrast to the alongshore distributions of phase difference, estimated amplitude of each frequency component of shoreline fluctuations did not show clear evidence of standing waves. This may be because of the deterioration of accuracy in estimation of spatial locations especially in the camera-far field. In the case of T=34s, for example, step-like phase distribution also indicates the partial standing waves and corresponding amplitude distribution relatively near the camera, i.e., Y < 200m, surely shows clear decay around the step of
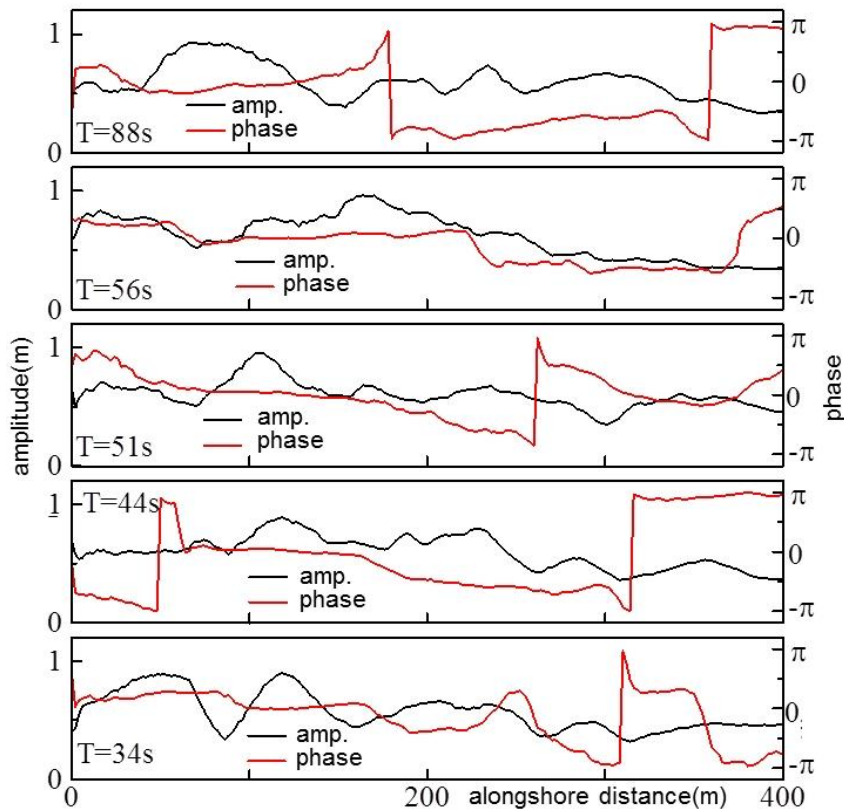

Figure 11 Alongshore distributions of amplitude and phase of shoreline fluctuation components at several frequencies.

phase difference where should be a node of partial standing waves. This alongshore variation of the amplitude however could not be clearly found in the camera-far field, Y>200m. This feature suggests that use of multiple cameras may improve the data accuracy both in phase and amplitude estimations. It should also be noted that accuracy of frequency and phase difference information is not significantly deteriorated even in the camera-far field and thus can be good indicators to capture the alongshore behaviors of infragravity waves.

Under the assumption that these infragravity wave components are propagating in the alongshore direction, wave length of each frequency component can be estimated from Fig. 11. Fig. 12 shows estimated wave length of each frequency components of shoreline fluctuations as a function of corresponding wave period. Fig. 12 also shows the dispersion relationship of edge waves of 0th and 1st modes in solid lines. Bottom slope of $\tan\beta=1/30$ was used for estimation of the dispersion relationship of edge waves. As seen in the figure, obtained wave length and corresponding wave period reasonably agree with dispersion relationships of edge wave. It is also seen from the figure that shoreline fluctuations of $T=88$s fit with dispersion relationship of 0th mode edge waves while other frequency components fit better with dispersion relationship of 1st mode edge wave. These analysis surely support the assumption that observed infragravity waves surely propagate in the alongshore directions and some of these component form standing waves, which may be resonantly amplified under certain conditions.

CONCLUSIONS

This study developed image-based monitoring techniques focusing on behavior of infragravity waves around the swash zone. Validity of proposed methodologies was tested both in laboratory experiment and in the actual field. This study especially focused on the use of succeeding multiple images for investigations of the characteristics of time-varying shoreline fluctuations. It was found through the laboratory experiment that behaviors of low-frequency components of observed shoreline fluctuations correspond to those of infragravity wave components in the swash zone.

The same procedures were applied to the Seisho coast where succeeding still images of the swash zone under stormy waves and daily wave conditions were captured by a field camera. Obtained images were rectified to obtain quantitative cross-shore fluctuations of the shoreline. Spectral analysis of obtained shoreline fluctuations clearly showed the evidence of infragravity waves. Dominant frequency of these infragravity wave components surely corresponded to those observed offshore by the wave gauge. Image-based monitoring technique enabled us to obtain fluctuations of instantaneous shoreline profiles over 400m-stretch along the coast. Based on obtained high resolution spatial and temporal variation of the shoreline, alongshore distributions of amplitude and phase difference of shoreline fluctuations were extracted and compared. Comparisons of these alongshore distributions indicate that infragravity waves propagate in the alongshore direction and some frequency components show behavior of standing waves while some other components show behaviors of progressive or partial standing waves. Estimated wave length of these infragravity waves were finally compared to the dispersion relationships of edge waves and good agreement of estimated wave length with dispersion relationship of edge waves also supports the evidence of infragravity waves propagating in the alongshore direction.
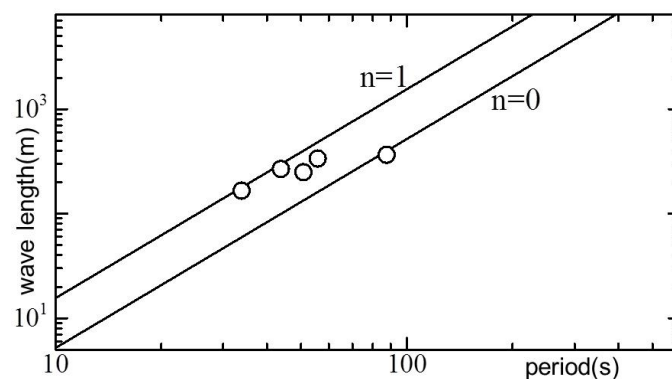

Figure 12 Dispersion relationship of edge wave (solid line) and observed shoreline fluctuations with specific dominant frequency components.

REFERENCES

Kato, K. 1981. Analysis of edge waves by means of empirical eigenfuctions, *Report of the Port and Harbour Research Institute*, vol.20, No.3, pp.3-52 (in Japanese).

Ranasinghe, R.S., Y. Fukase, S. Sato and Y. Tajima. 2011. Local concentration of waves due to alongshore variation of nearshore bathymetry, *Coastal Engineering Journal*, 53, 3, 201-222.

Sato, S. Kosugi, T., Kato, K. and T. Kuchiishi. 1998. Field Investigation of Coastal Damages on Seishoh Coast Caused by Typhoon 9720, *Proc. of Coastal Eng.*, JSCE, vol.45, pp.326-330. (in Japanese)

Seki, K., and Y. Mizuguchi. 2008. Shoaling of long period waves induced by grouping short-waves on sloping bottom. *Journal of the Japan Society of Civil Engineers B*, JSCE, vol.64, 62-70 (in Japanese).

Tajima, Y., H. Liu and S. Sato : Dynamic changes of waves and currents over the collapsing sandbar of the Tenryu river mouth observed during Typhoon T0704, *Proc. of Coastal Dynamics* 2009, CD-ROM published by World Scientific.

Tajima, Y. and S. Sato. 2009. Numerical investigations of locally concentrated damages on Seisho coast sue to typhoon T0709, *Proc. of 5th Int. Conf. on Asian and Pacific Coasts*.

Tajima, Y. and S.Sato. 2010. Local concentration of slowly varying wave and current fields around the abruptly changing bottom slopes along the shore, *Proc. of 32nd Int. Conf. on Coast. Eng.*, doi: http://dx.doi.org/10.9753/icce.v32.waves.21